

Charge and orbital orderings associated with metal-insulator transition in V_6O_{13} T. Toriyama,¹ T. Nakayama,¹ T. Konishi,² and Y. Ohta^{1,*}¹*Department of Physics, Chiba University, Chiba 263-8522, Japan*²*Graduate School of Advanced Integration Science, Chiba University, Chiba 263-8522, Japan*

(Received 3 March 2014; revised manuscript received 8 August 2014; published 21 August 2014)

Density-functional-theory-based electronic-structure calculations are carried out to elucidate the mechanism of the metal-insulator transition (MIT) of a Wadsley-phase vanadium oxide V_6O_{13} . We show that, at the MIT, the orbitals occupied by electrons are reconstructed in the single trellis layers of the V(1) ions, which occurs simultaneously with the transfer of electrons from the V(2) to V(3) ions in the double trellis layers, leaving the V(2) ions nonmagnetic. We discuss that these changes lead to the formation of spin-singlet state associated with the ordering of the d_{yz} and d_{xz} orbitals in the V(1) zigzag chain, together with the formation of the Mott-insulator state with frustrated spin degrees of freedom in the zigzag ladder of the d_{xy} orbitals of the V(3) ions; possible antiferromagnetic ordering patterns are predicted for the latter state. Thus, the spin-singlet and antiferromagnetic states coexist in spatially separated regions at lowest temperatures. The band Jahn-Teller-type instability hidden in the single trellis layer, which is the orbital ordering instability in the strong correlation limit, is suggested to cause the MIT.

DOI: [10.1103/PhysRevB.90.085131](https://doi.org/10.1103/PhysRevB.90.085131)

PACS number(s): 71.30.+h, 75.25.Dk, 71.20.-b

I. INTRODUCTION

The elucidation of mechanisms of the metal-insulator transition (MIT) has long been one of the central issues in physics of strongly correlated electron systems [1]. A Wadsley-phase vanadium oxide V_6O_{13} is one of such systems where the mechanism of the MIT is not yet known [2–9]. This oxide material is paramagnetic metallic at high temperatures and undergoes the first-order MIT at 150 K. The structural distortion occurs at the transition [5,9], which is associated with a sudden decrease in the uniform magnetic susceptibility [4,6,8], and by further lowering temperature, the antiferromagnetic long-range order appears below 55 K [4,6].

The crystal structure of V_6O_{13} is composed of the two-dimensional (2D) single and double trellis layers [5,10–12] (see Fig. 1), where the V ions are in a mixed valence state with an average valence of $V^{4.33+}$ ($3d^{0.66}$); i.e., there are formally V^{5+} ($3d^0$) and V^{4+} ($3d^1$) ions in a 1 : 2 ratio. It has recently been established that the structural phase transition, which is associated with the MIT, occurs from a high-temperature monoclinic phase (space group $C2/m$) to a low-temperature monoclinic phase (space group Pc) [12], whereby earlier reports [5,11] on the low-temperature crystal structure have been corrected.

The electric resistivity was reported to show a quasi-one-dimensional (1D) electron conduction at temperatures above the MIT and therefore this material was thought to be a quasi-1D electric conductor [9]. However, recent experimental data [13] indicate that it has the metallic temperature dependence in all directions of the crystal axes above the MIT although it exhibits a rather strong anisotropy ($\rho_a = 0.032$, $\rho_b = 0.0023$, and $\rho_c = 0.47$ Ω cm at 300 K). The electron conduction of this material is thus much more three dimensional (3D) than previously thought. The MIT temperature decreases by applying pressure, which is ~ 100 K at 1.4 GPa [13]. So far, a number of studies including

the photoemission spectroscopy [14,15], angle-resolved photoemission spectroscopy (ARPES) [16,17], as well as the band-structure calculations [18] have been performed, but the mechanism of the MIT of this material is not yet clear.

In this paper, motivated by such developments in the field, we carry out the density-functional-theory- (DFT-) based electronic-structure calculations to clarify the electronic structure of V_6O_{13} and, using the results, we discuss the mechanisms of the MIT and antiferromagnetic transition of this material. We will first show for the high-temperature metallic phase that an electron is located largely on the d_{xz} orbital of V(1) with a substantial admixture of the d_{yz} orbital and that other two electrons are located largely on the d_{xy} orbitals of V(3) with a significant contribution from the d_{xy} orbitals of V(2), where the x , y , and z axes are defined in Fig. 1 and are used throughout the paper. As a consequence, two nearly degenerate bands coming from the d_{xy} orbitals of V(2) and V(3) form two pairs of the quasi-1D Fermi surfaces and a band coming from the d_{yz} orbital of V(1) form a quasi-2D-like Fermi surface. Then, for the low-temperature insulating phase, we will show the following: There appears the band gap of the size ~ 0.2 eV [7,17]. Redistribution of electrons occurs at the MIT, which leads to the formal oxidation states of V^{4+} ($3d^1$) for the V(1) and V(3) ions and V^{5+} ($3d^0$) for the V(2) ions. Consequently, an electron is localized on each of the d_{xz} orbital of V(1a) and d_{yz} orbital of V(1b) in the single trellis layer, and an electron is localized on each of the d_{xy} orbitals of V(3a) and V(3b) in the double trellis layer. This system therefore offers an example of the MIT that occurs with the redistribution of electrons, which is unique in systems with more than one structural building block, just as in β - $Na_{0.33}V_2O_5$ [19,20].

We will thereby discuss consequences of the MIT of V_6O_{13} as follows: The two electrons on the neighboring V(1) ions in the single trellis layer, on the one hand, form the spin-singlet state associated with orbital ordering and suppress the spin excitations at temperatures below the MIT. The electrons on the d_{xy} orbitals of the V(3a) and V(3b) ions in the double trellis layers, on the other hand, undergo a Mott transition to form the quasi-1D zigzag ladders of $S = \frac{1}{2}$ spins. The spin degrees of

*ohta@faculty.chiba-u.jp

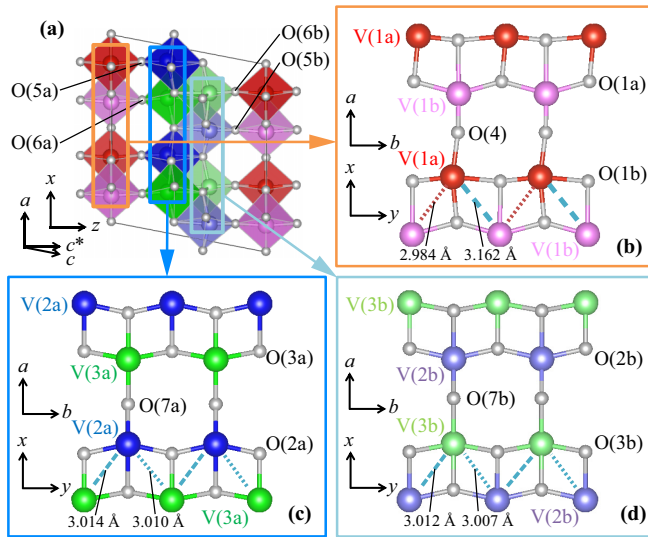


FIG. 1. (Color online) Schematic representations of the crystal structure of the low-temperature phase of V_6O_{13} (Ref. [12]). We show the side view of the single and double trellis lattices in (a), top view of the single trellis layer in (b), and top view of each of the double trellis layers in (c) and (d). For the high-temperature phase, where the structural distortion is absent, V(1a) and V(1b) become equivalent and are replaced by V(1), V(2a) and V(2b) by V(2), and V(3a) and V(3b) by V(3), and the same is done for the O ions, except O(4) where “O(4a)” and “O(4b)” are equivalent. The a and c (c^*) axes are for the high-temperature phase [10], which are interchanged in the low-temperature phase [12]. The x , y , and z axes shown are used for both the high-temperature and low-temperature phases throughout the paper.

freedom of this zigzag ladder are strongly frustrated resulting in some experimental consequences, but at temperatures below 55 K, the antiferromagnetic long-range order occurs as the experimental data indicate [4,6], for which we will predict three possible ordering patterns. Thus, the spin-singlet and antiferromagnetic states coexist in spatially separated regions of the material at lowest temperatures. A possible scenario for the mechanism of the MIT in the present system will be suggested.

This paper is organized as follows: In Sec. II, we will briefly present our method of calculations. In Sec. III, we will show our results of calculations for both the high- and low-temperature phases of V_6O_{13} and discuss the charge and orbital orderings, spin degrees of freedom at low temperatures, as well as the mechanism of the MIT of V_6O_{13} . Our work will be summarized in Sec. IV.

II. METHOD OF CALCULATION

We employ the WIEN2K code [21] based on the full-potential linearized augmented-plane-wave method and present the calculated results obtained in the generalized gradient approximation (GGA) for electron correlations. We take into account the Hubbard-type repulsive interaction (GGA + U) to improve the description of electron correlations in the V $3d$ orbitals. Here, we use the rotationally invariant version of the GGA + U method with the double-counting correction

in the fully localized limit [22,23]. We choose a standard value $U = 3.5$ eV, which reproduces the experimental band gap in the insulating phase [7,17]. The values $U = 3$ –8 eV are also tested to see the characters of the bands clearly. We use the exchange-correlation potential of Ref. [24]. The spin-orbit interaction is not taken into account and the spin polarization is allowed when necessary. Note that the vanadium oxide materials are the typical strongly correlated electron system and it is often rather hard to account for their MIT in the framework of GGA or local-density-approximation (LDA) type of calculations, for which the LDA or GGA combined with the dynamical mean-field theory (DMFT), i.e., the LDA + DMFT approach [25–29], as well as the use of modern functionals such as a modified Becke-Johnson exchange potential [30] have recently been shown to be useful. However, in this work, we instead adopt the cheapest approach of GGA + U and consider the calculated results in comparison with the available experimental data to deduce the essential physics hidden in the system.

We use the crystal structure and atomic positions measured by Wilhelmi *et al.* [10] at 298 K for the high-temperature metallic phase and those measured by Höwing *et al.* [12] at 95 K for the low-temperature insulating phase. The crystal structure of the high-temperature metallic phase has the monoclinic symmetry ($C2/m$ space group) with the monoclinic angle of $\beta = 100.87^\circ$ and lattice constants of $a = 11.922$, $b = 3.680$, and $c = 10.138$ Å at 298 K [10]. The primitive unit cell contains 6 V ions and 13 O ions, with 3 inequivalent V sites and 7 inequivalent O sites (see Fig. 1). The crystal structure of the low-temperature insulating phase has the monoclinic symmetry (Pc space group) with the monoclinic angle of $\beta = 100.927^\circ$ and lattice constants of $a = 10.0605$, $b = 3.7108$, and $c = 11.9633$ Å at 95 K [12]. The primitive unit cell contains 12 V ions and 26 O ions, with 6 inequivalent V sites and 13 inequivalent O sites (see Fig. 1).

In the self-consistent calculations, we use 513 k points (60 k points) in the irreducible part of the Brillouin zone for the high-temperature (low-temperature) phase. Muffin-tin radii (R_{MT}) of 1.64 and 1.46 bohrs are used for V and O ions, respectively, and the plane-wave cutoff of $K_{max} = 7.00/R_{MT}$ is assumed. We use the codes VESTA [31] and XCRYSDEN [32] for graphical purposes.

III. RESULTS AND DISCUSSION

A. High-temperature metallic phase

First, let us discuss the calculated results for the high-temperature metallic phase of V_6O_{13} . Calculated results for the partial density of states (DOS) indicate that the O $2p$ states, V $3d t_{2g}$ states, and V $3d e_g$ states are located mainly in the energy ranges of $-7.5 \lesssim \varepsilon \lesssim -2.2$ eV, $-0.7 \lesssim \varepsilon \lesssim 2.1$ eV, and $2.1 \lesssim \varepsilon \lesssim 5.4$ eV, respectively [see Fig. 2(a)]. There appears a gap of ~ 1.5 eV between the O $2p$ and V $3d t_{2g}$ states and the Fermi level is located near the bottom of the V $3d t_{2g}$ states. In the t_{2g} manifold, near the Fermi level in particular, the hybridization with the O $2p$ orbitals is seen not to be very strong.

Calculated results for the band dispersions and Fermi surfaces are shown in Fig. 3, where we assume the value

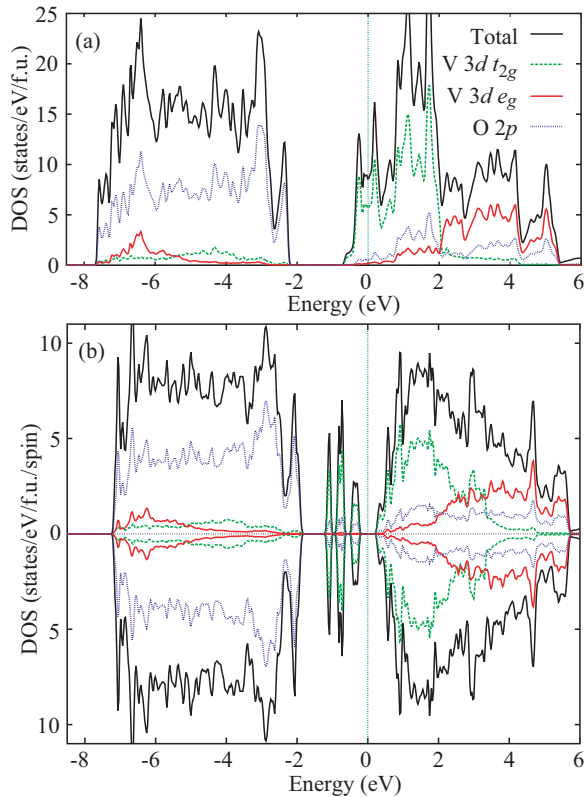


FIG. 2. (Color online) Calculated total and partial DOSs (per formula unit, f.u.) for (a) the high-temperature paramagnetic metallic phase and (b) low-temperature antiferromagnetic insulating phase of V_6O_{13} . In (b), the upper and lower panels display the up- and down-spin DOSs, respectively. The vertical line indicates the Fermi level. We assume the value $U = 3.5$ eV.

$U = 3.5$ eV. We find that there are four bands near the Fermi level: the lowest band comes mainly from the d_{xz} and d_{yz} orbitals of V(1) and is located well below the Fermi level, the second and third bands come mainly from the d_{xy} orbitals of V(2) and V(3) and cross the Fermi level, and the fourth band comes mainly from the d_{yz} orbital of V(1) and also crosses the Fermi level. The middle two bands have two pairs of the quasi-1D sheet-like Fermi surfaces but the fourth band is less quasi-1D-like. Note that the highly anisotropic 3D-like electron conduction observed in the temperature dependence of the electric resistivity [13] is consistent with the result at $U = 3.5$ eV. The unusually large U values, such as $U \simeq 8$ eV, are required if the quasi-1D electron conduction [9] is in reality because, in this case, the fourth band entirely shifts above the Fermi level and at the same time the two pairs of the quasi-1D-like bands become more 1D like.

The calculated results for the band dispersions can be compared with the results of the experimental ARPES spectra [16,17], where two spectral features have been observed, i.e., a less dispersive spectral weight located ~ 0.8 eV below the Fermi level and a dispersive spectral weight crossing the Fermi level with the Fermi momentum of $k_F b / \pi = 0.29 \pm 0.01$ [16]. Our calculated results are roughly consistent with these experimental data in that there are electron Fermi sheets at the Γ point of the Brillouin zone and there is the less dispersive

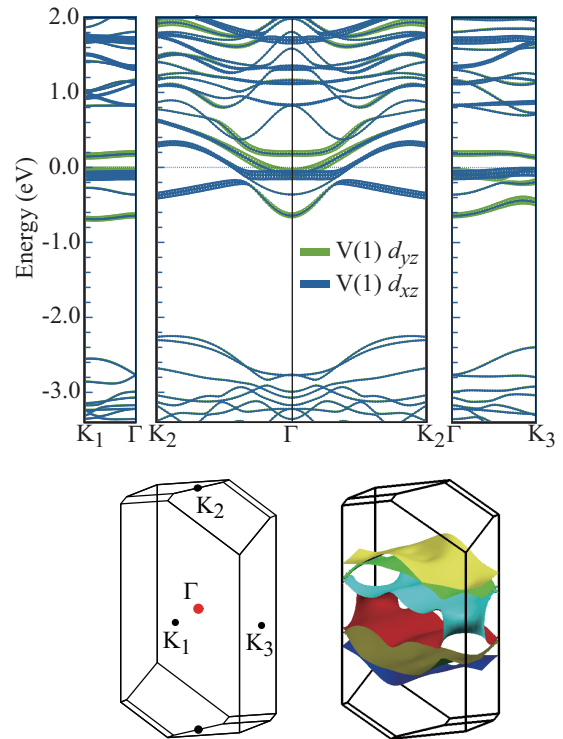


FIG. 3. (Color online) Calculated band dispersions (upper panel) and Fermi surfaces (lower panel) in the high-temperature metallic phase of V_6O_{13} . In the band dispersions, the widths of the curves are drawn in proportion to the weights of the d_{yz} and d_{xz} orbitals of the V(1) ions. The horizontal line indicates the Fermi level. We assume the value $U = 3.5$ eV.

spectral weight ~ 0.5 eV below the Fermi level. Quantitatively, however, the agreement is not satisfactory. At $U \simeq 3.5$ eV, the fourth band coming from the d_{yz} orbital of the V(1) ions clearly crosses the Fermi level, so that there are three bands that cross the Fermi level. In this case, we may suppose that the experimental spectral weight comes from these three bands with nearly the same Fermi momenta around $\sim 0.3\pi/b$ that could not be resolved in the experimental accuracy. Our calculated results are consistent with the ARPES experiment in this sense. If we assume $U = 8$ eV, there are only two bands that cross the Fermi level. In this case, the experimental Fermi momentum is too small to be consistent with the numbers of electrons in the system: i.e., the Fermi momentum should be at $\sim 0.5\pi/b$, rather than the ARPES data of $\sim 0.29\pi/b$ [16]. Further experimental studies for resolving these puzzles, in particular for the detection of the four bands near the Fermi level and quasi-2D-like Fermi surfaces predicted here, are highly desirable.

The distribution of the 3d electrons among the three V ions is calculated and the numbers of electrons inside the muffin-tin spheres obtained at $U = 3.5$ eV are listed in Table I; the results do not depend strongly on the U values used. Although the calculated results do not well correspond to the experimental valence states by definition, we find that the tendencies are reasonably consistent with experimental assignment of the formal valence states [6,8–10,33] that the V(2) ions are more 5+ like and the V(1) and V(3) ions are more 4+ like although

TABLE I. Calculated numbers of V $3d$ t_{2g} electrons in the muffin-tin spheres for the high-temperature metallic phase of V_6O_{13} . The e_g contributions are negligibly small. $U = 3.5$ eV is assumed.

	$3d^{tot}$	$3d_{xy}$	$3d_{yz}$	$3d_{xz}$
V(1)	0.608	0.002	0.227	0.378
V(2)	0.268	0.108	0.085	0.063
V(3)	0.415	0.268	0.077	0.058

they are not complete. The bond valence sums given in Table II calculated using the experimental bond lengths [10] also show the same tendency. The orbital occupations of electrons in the V ions are calculated and are also given in Table I. We find that the occupied orbitals are predominantly d_{xz} like with a strong admixture of d_{yz} for V(1) and that they are predominantly d_{xy} like for V(2) and V(3). These results are not very sensitive to the U values used and are consistent with results of the recent NMR experiment [33]. These t_{2g} orbitals of the V ions are hybridized weakly with the respective $2p$ orbitals of the O ions near the Fermi level, which are $2p_z$ like for O(1) and $2p_x$ like for O(3).

B. Low-temperature insulating phase

Next, let us discuss the low-temperature insulating phase. Since the band-structure calculations based on the GGA + U and similar types of approximations cannot reproduce the paramagnetic Mott insulating phase without symmetry breaking, we assume possible antiferromagnetic orderings in the calculation and consider the results to find a real electronic state of the system. In V_6O_{13} , the antiferromagnetic long-range order is confirmed in experiment below 55 K but its spatial pattern is not experimentally known [4,6]. Here, we extend the unit cell twice as large as the unit cell of the observed low-temperature crystal structure [12] along the b axis and search for insulating solutions with any antiferromagnetic ordering consistent with available experimental data.

We then find three low-energy solutions, all of which have nearly the same spatial pattern of the charge and orbital states, but have different spatial patterns of the antiferromagnetic spin polarization. The total energies of these solutions are -6674.38765 , -6674.38752 , and -6674.38743 Ryd/f.u.. The presence of the states with nearly degenerate total energies suggests the frustrated nature in the spin degrees of freedom of the system, which may play an important role in the insulating phase of this material. This aspect will be discussed in Sec. III C. We here discuss the charge and orbital states;

TABLE II. Calculated bond valence sums of the V ions in the high-temperature metallic (upper table) and low-temperature insulating (lower table) phases of V_6O_{13} , where the experimental bond lengths [10,12] are used.

	V(1)	V(2)	V(3)			
	4.37	4.65	4.14			
	V(1a)	V(1b)	V(2a)	V(2b)	V(3a)	V(3b)
	4.33	4.24	4.61	4.69	4.27	4.20

only the lowest-energy solution is discussed because the three low-energy solutions have nearly equivalent charge and orbital states.

The calculated results for the total and partial DOS of the lowest-energy solution are shown in Fig. 2(b) and their orbital decompositions are shown in Fig. 4. We first find that the band gap of the size ~ 0.3 eV opens at $U = 3.5$ eV, which is consistent with experiment [16]. We also find that the lowest part of the t_{2g} bands is split off to form the narrow bands just below the Fermi level; three characteristic peaks appear in the DOS [see Fig. 2(b)]. As shown in Fig. 4, the lower and upper peaks come mainly from the d_{xz}^\uparrow orbital of V(1a) and d_{yz}^\downarrow orbital of V(1b), the splitting of which is due to the bonding-antibonding splitting of the neighboring d_{xz} and d_{yz} orbitals of the V(1a) and V(1b) ions with the same spin directions. The middle peak comes mainly from the d_{xy}^\downarrow orbital of V(3a) and d_{xy}^\uparrow orbital of V(3b). Here, we use the notion d^σ with $\sigma = \uparrow$ and \downarrow , indicating the up- and down-spin d orbitals, respectively.

The numbers of electrons on each orbital inside the muffin-tin sphere are listed in Table III, where we find that the values are consistent with the results of the partial DOS discussed above, i.e., the numbers of electrons on the d_{xz}^\uparrow orbital of V(1a), d_{yz}^\downarrow orbital of V(1b), as well as on the d_{xy}^\downarrow orbital of V(3a) and d_{xy}^\uparrow of V(3b) are significantly large. Small numbers of electrons in the d_{xy}^\downarrow orbital of V(2a) and d_{xy}^\uparrow orbital of V(2b) are also noticed. We also calculate the spatial distribution of electrons in the energy window of $-1.5 < \varepsilon < E_F$ (Fermi level); the result is shown in Fig. 5, where the charge and orbital ordering pattern of the t_{2g} electrons discussed above is clearly visible. A significant contribution from the $2p_z$ orbital of O(1a) is also noticed.

Based on these calculated results, we can describe the charge and orbital states in the low-temperature insulating phase as follows, whereby the charge redistribution and orbital reconstruction that occur with the MIT are clarified:

(i) The V(2a) and V(2b) ions are essentially in the formal valence state of $5+$ (or $3d^0$ state) though a small d_{xy} contribution can be identified, indicating that a considerable charge flow (or redistribution of electrons) occurs at the MIT temperature. This means that the V(1a), V(1b), V(3a), and V(3b) ions are essentially in the formal valence state of $4+$ (or $3d^1$) below the MIT, in agreement with the experimental assignment [6,8–10,33], as well as with the bond valence sums given in Table II calculated using the experimental bond lengths [12]. This phenomenon may be referred to as a charge ordering. Note that the charge flow between the structural building blocks adds complexity to the mechanism of the MIT, just as in β - $\text{Na}_{0.33}\text{V}_2\text{O}_5$ [19,20].

(ii) A single $3d$ orbital is predominantly occupied by an electron in the V(1a), V(1b), V(3a), and V(3b) ions: i.e., the d_{xz} orbital in V(1a), d_{yz} orbital in V(1b), and d_{xy} orbital in V(3a) and V(3b). Note that the occupation of the d_{xz} and d_{yz} orbitals of V(1) in the high-temperature metallic phase changes into the occupation of the d_{xz} orbital of V(1a) and d_{yz} orbital of V(1b) in the low-temperature insulating phase, the phenomenon of which may be referred to as an orbital ordering. We hope that our results thus obtained will be helpful for interpreting the results of a recent NMR experiment [33]. We point out here

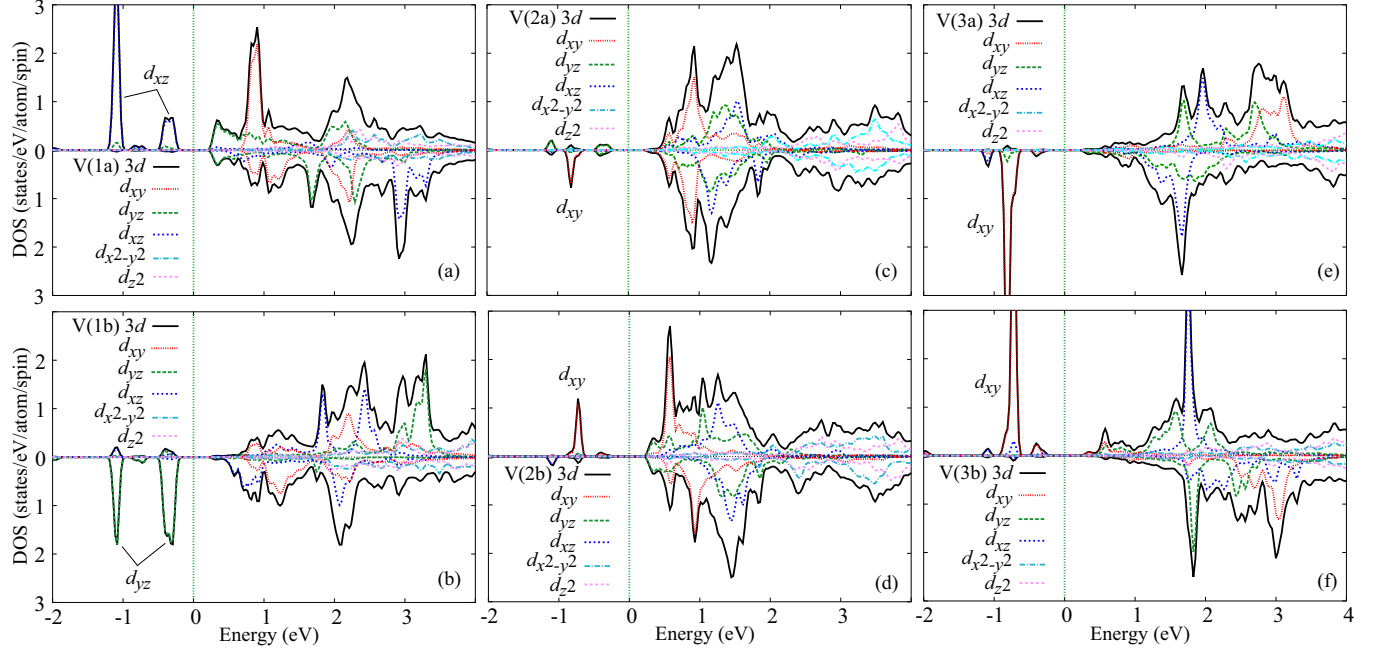


FIG. 4. (Color online) Calculated orbital-decomposed partial DOS in the low-temperature antiferromagnetic insulating phase of V_6O_{13} . (a) V(1a), (b) V(1b), (c) V(2a), (d) V(2b), (e) V(3a), and (f) V(3b), in each of which the upper and lower panels display the up- and down-spin DOSs, respectively. The vertical line indicates the Fermi level. $U = 3.5$ eV is assumed.

that the present result is in contrast to the orbital occupation of a single-trellis-lattice compound α' - NaV_2O_5 [34–37], where the d_{xy} orbitals of V ions on each rung of the ladder are occupied by one electron per rung; the crystal field in the pyramidal coordination of ligand oxygens causes the difference.

Note that, since the d_{xz} and d_{yz} orbitals of the V(1) ions are not exactly degenerate in the high-temperature metallic phase, the Jahn-Teller-type mechanism for the orbital ordering and lattice distortion cannot simply be applicable. We will suggest a possible scenario for the mechanism of the MIT of this material in Sec. III D.

C. Spin degrees of freedom

Now, let us discuss the spin degrees of freedom in the low-temperature insulating phase of V_6O_{13} . First, we consider the spin state of the V(1) ions. Based on the results of our GGA + U calculations, we may assume that an electron is localized on each V(1) ion, thereby forming a spin $S = \frac{1}{2}$ zigzag chain of the localized electrons on the d_{xz} orbital of V(1a) and d_{yz} orbital of V(1b) in the low-temperature insulating phase [see Fig. 5(a)]. Then, the experimental structural data [12] indicate that the zigzag chain composed of the V(1a) and V(1b) ions shows a strong bond alternation below the MIT temperature: the bond length between the neighboring V(1a) and V(1b) ions is 3.047 Å in the high-temperature metallic phase, whereas in the low-temperature insulating phase, a shorter bond with length 2.984 Å and a longer bond with length 3.162 Å alternate [see Fig. 1(b)]. Thus, we may anticipate that the spin-singlet state, rather than the antiferromagnetic ordering obtained in our GGA + U calculation, is actually formed between the $S = \frac{1}{2}$ spins on the d_{xz} and d_{yz} orbitals of the neighboring V(1a) and V(1b) ions,

as is illustrated in Fig. 6(a). Also, the coupling between the two zigzag chains of the V(1) ions is small because the d_{xz} orbital of V(1a) and d_{yz} orbital of V(1b) in the neighboring zigzag chains are orthogonal to each other [see Fig. 5(a)].

The spin-singlet formation thus obtained leads to suppression of the low-energy spin excitations and is therefore consistent with the observed sudden decrease in the uniform magnetic susceptibility at the MIT [4,6,9]. The exchange coupling between the two V(1) ions may be caused not only by the second-order process of the direct hopping of electrons between the d_{xz} and d_{yz} orbitals, but also by the fourth-order process via the p_z orbital of the O(1a) ions, as we notice a significant p_z contribution in Fig. 5(a). Note that the spin-singlet formation in the spin- $\frac{1}{2}$ chain of the V(1) ions may contribute to the gain in energy via the bond alternation of the chain, as in the spin-Peierls mechanism. In the present case, however, this may work cooperatively with the localization of electrons caused by the electronic instability hidden in the single trellis layer, as we will discuss in Sec. III D.

TABLE III. Calculated numbers of V 3d t_{2g} electrons with spin σ ($= \uparrow, \downarrow$) in the muffin-tin spheres for the low-temperature antiferromagnetic insulating phase of V_6O_{13} . The e_g contributions are negligibly small. $U = 3.5$ eV is assumed.

	$3d^{\text{tot}}$	$3d_{xy}^{\uparrow}$	$3d_{xy}^{\downarrow}$	$3d_{yz}^{\uparrow}$	$3d_{yz}^{\downarrow}$	$3d_{xz}^{\uparrow}$	$3d_{xz}^{\downarrow}$
V(1a)	0.499	0.000	0.000	0.029	0.002	0.461	0.007
V(1b)	0.546	0.000	0.000	0.021	0.489	0.028	0.008
V(2a)	0.138	0.001	0.094	0.008	0.006	0.023	0.006
V(2b)	0.140	0.097	0.001	0.007	0.007	0.006	0.022
V(3a)	0.540	0.001	0.484	0.003	0.001	0.009	0.042
V(3b)	0.562	0.505	0.001	0.001	0.003	0.044	0.008

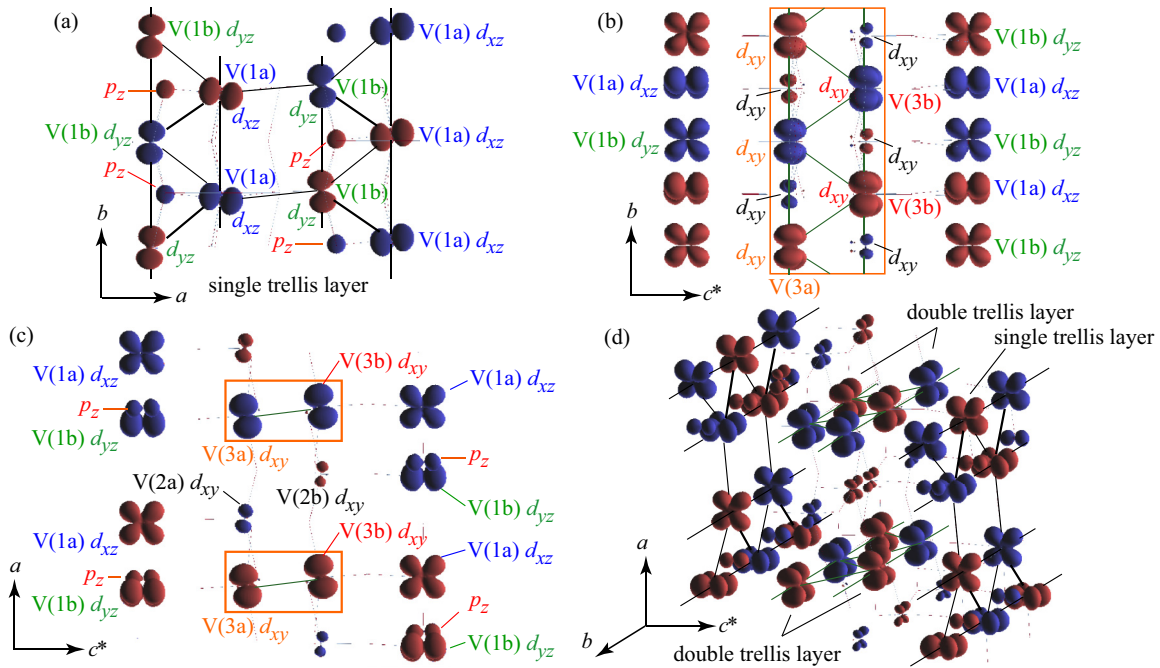


FIG. 5. (Color online) Calculated spatial distribution of electrons in the energy window between -1.5 eV and $E_F = 0$ eV for the lowest-energy solution in the low-temperature insulating phase of V_6O_{13} , where an isovalue of 0.012 electrons/bohrs³ is used and $U = 3.5$ eV is assumed. The orbitals occupied by electrons are clearly visible. The color distinguishes the electron spins. The distribution is (a) viewed down the c^* axis (for the single trellis layer), (b) viewed down the a axis, (c) viewed down the b axis, and (d) viewed from the rotated angle. The squares in (b) and (c) mark the zigzag ladder emerging in the double trellis layer.

Next, we consider the spin state of the V(3) ions. Because we may assume that the electrons on the V(1) ions form the spin-singlet state and the V(2) ions are nonmagnetic (or in the $3d^0$ state) as discussed above, a pair of the V(3) chains running along the b axis, which is a zigzag ladder of the d_{xy} orbitals of the V(3a) and V(3b) ions, emerges as a spatially isolated structural block. This is actually evident in the calculated electron density distribution shown in Fig. 5(b); the localized

electrons on the d_{xy} orbitals of the V(3a) and V(3b) ions form the 1D spin- $\frac{1}{2}$ zigzag ladder running along the b direction of the crystal axis.

To consider the spin state of this zigzag ladder, we can estimate the exchange coupling constants between the neighboring V(3) ions using the total energies of various antiferromagnetic solutions in principle. We in fact find from the total energies of the three antiferromagnetic solutions that although the results are not quantitatively reliable, they are all antiferromagnetic with comparable strength, suggesting the presence of spin frustration. Note that the temperature dependence of the uniform magnetic susceptibility measured in the low-temperature phase above the antiferromagnetic ordering temperature [9] is consistent with the theoretical results calculated for the frustrated zigzag Heisenberg ladder [38]. Note also that, unlike in the V(1) zigzag chain, the bond alternation along this zigzag chain is negligibly small, i.e., the measured bond lengths are 3.239 and 3.240 Å (which may be compared with the bond length 3.711 Å along the legs of this zigzag ladder) [12]. Therefore, the spin degrees of freedom of this zigzag ladder are strongly frustrated, so that the antiferromagnetic ordering is significantly suppressed. This situation is illustrated in Fig. 6(b).

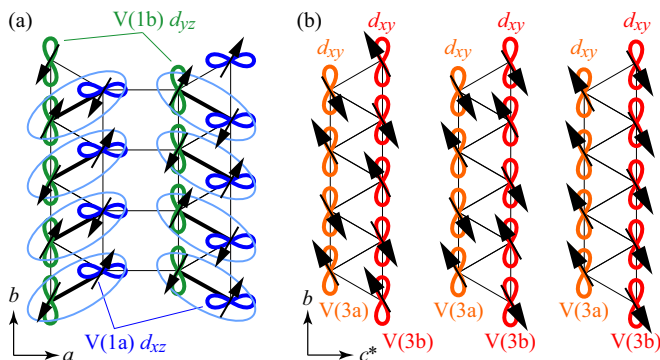


FIG. 6. (Color online) Schematic representations of the spins on (a) the zigzag ladder of the V(1a) and V(1b) ions in the single trellis layer and (b) the zigzag ladder of the V(3a) and V(3b) ions in the double trellis layer. In (a), the spin-singlet state is marked by a large ellipse. In (b), three possible ordering patterns of spins are illustrated by arrows. Only the relative orientation of spins is meaningful here because the magnetic anisotropy is not taken into account in the calculations although experimentally the direction of antiferromagnetic spin is parallel to the b axis [6].

We should point out here that the ground state of the pure 1D zigzag Heisenberg (or Hubbard) ladder has been under intense theoretical debate [39], suggesting the presence of incommensurate spiral spin correlations [40], but in the present case, there is a weak 3D (or quasi-2D) exchange coupling between the zigzag ladders in the 3D crystal structure, and therefore, any antiferromagnetic long-range order may be realized at the lowest temperatures, depending on the strength

of the exchange interactions. In our GGA + U calculation, where only the collinear spin states are taken into account, the lowest-energy antiferromagnetic pattern is found to be the one shown in Fig. 5. Note that if there were no spin frustrations in this system, the antiferromagnetic phase transition would occur simultaneously with the MIT. In this respect, the experimental determination of the antiferromagnetic ordering pattern in V_6O_{13} at the lowest temperatures using, e.g., the neutron scattering experiment, are highly desirable. The observation of the low-energy spin excitations in the frustrated zigzag ladders above the antiferromagnetic transition temperature, which may detect the incommensurate spiral spin correlations, should also be an interesting issue in the present system.

D. Possible mechanism of the MIT

Finally, let us consider the mechanism of the MIT of this material. The band-gap opening, lattice distortion, charge

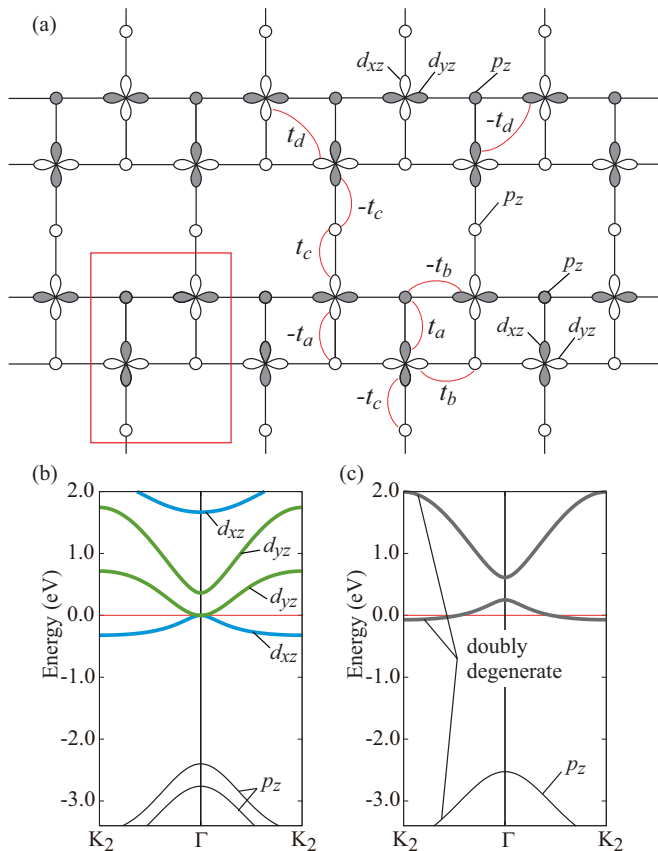


FIG. 7. (Color online) (a) Schematic representations of the orbitals near the Fermi level in the single trellis layer. A large square indicates the unit cell. (b) The tight-binding band dispersions of the isolated single trellis layer in the high-temperature metallic phase. The values of the onsite energies and hopping parameters used are $\varepsilon_p = -2.4$, $\varepsilon_d = 0.0$, $t_a = 1.0$, $t_b = 1.1$, $t_c = 1.7$, and $t_d = 0.2$ in units of eV. The horizontal line indicates the Fermi level. (c) The tight-binding band dispersions of the isolated zigzag ladder of the single trellis layer in the high-temperature metallic phase, which are obtained by setting $t_c = 0$. The three bands shown are all doubly degenerate because the zigzag chain indicated by the shaded orbitals in (a) is equivalent to the zigzag chain indicated by the unshaded orbitals.

ordering, orbital ordering, and spin-singlet formation, all of which occur simultaneously at the MIT temperature, have to be explained on the basis of the calculated results shown above with the help of available experimental data. The antiferromagnetic ordering that occurs at the lower temperature also has to be explained consistently. Although rather speculative, we may suggest the following scenario.

We first consider the band structure of the single trellis layer in the high-temperature metallic phase, where the relevant orbitals near the Fermi level are illustrated in Fig. 7(a). We then determine the tight-binding band parameters to reproduce approximately the GGA + U band dispersions coming from the single trellis layer given in Fig. 3. The resultant tight-binding band dispersions are shown in Fig. 7(b), which reproduce the original band dispersions reasonably well. There are four d and two p bands because the unit cell contains four d and two p orbitals as shown in Fig. 7(a). The lowest-energy d band is filled with two electrons (per unit cell); a slight shift of the Fermi level caused by the charge flow is assumed in the following discussions. We thus confirm that no noticeable instabilities that may cause the MIT are present in the band dispersions of the single trellis layer.

Let us then hypothetically cut the hopping parameter that connects between the zigzag ladders in the single trellis layer, i.e., set $t_c = 0$. The band dispersions in the resultant isolated zigzag ladder thus obtained are shown in Fig. 7(c). We find that there appear doubly degenerate bands that cross the Fermi level; the degeneracy appears because the zigzag chain consisting of the shaded d_{xz} and d_{yz} orbitals in Fig. 7(a) is equivalent to the zigzag chain consisting of the unshaded d_{xz} and d_{yz} orbitals, and these two zigzag chains are orthogonal to each other in the single zigzag ladder, even in the presence of the p_z orbitals of O ions. This degeneracy, which is inherent in the single zigzag ladder, therefore leads to the band Jahn-Teller-type instability of the system. Assume here that the lattice distortion creating the level splitting between the d_{xz} and d_{yz} orbitals of the V ions is introduced and that the effect is strong enough, then the degeneracy is lifted to split the bands into two, such that the lower band is filled with two electrons. This is the orbital-ordered state, which can be semiconducting in the noninteracting limit. This system can, however, be Mott insulating if the onsite Coulomb interaction is strong enough. Thus, the orbital ordering of the localized electrons is realized with the help of the lattice distortion. The resultant system is the so-called Δ chain [41] of $S = \frac{1}{2}$ spins [see the shaded orbitals shown in Fig. 7(a)], where the bond alternation along the zigzag chain may also occur, as in the real material, due to the spin-singlet formation by the spin-Peierls-like mechanism. The spatial pattern of this orbital ordering is the one shown in Fig. 5(a), where we note that the two orbitals connecting the two zigzag ladders are indeed orthogonal to each other, even in the presence of the p_z orbital of O(4), which in turn cuts the hopping parameters between the two zigzag ladders. We may therefore state that the MIT of this material is due to the band Jahn-Teller-type instability hidden in the zigzag ladder of the single trellis layer, which leads to the orbital ordering associated with the lattice distortion.

Alternatively, we may begin with the limit of strong electron correlations. Suppose that the (nearly) degenerate d_{xz} and d_{yz} orbitals are present on the V ions in the

limit of vanishing hopping parameters, then the fourth-order perturbation processes of hopping of an electron via the p_z orbital of the O ions, i.e., t_a and t_b , yield the gain in kinetic energy, resulting in the antiferromagnetic exchange interactions between two electrons on the d_{xz} and d_{yz} orbitals of the neighboring V(1) ions. A simple counting of the numbers of the hopping processes then indicates that the orbital ordering pattern shown in Fig. 7(a) acquires the largest energy gain. This is also the case when we consider the largest direct d_{xz} - d_{yz} hopping processes via t_d . The spatial pattern of the orbital ordering thus obtained is again the one shown in Fig. 5(a). Note that the exchange interaction between the two zigzag ladders via t_c is ferromagnetic if we take into account the Hund's rule coupling between two electrons on the d_{xz} and d_{yz} orbitals of the V(1) ions, which however does not affect the obtained orbital-ordering pattern in the single trellis layer. The lattice may be deformed as in the real material by the spin-Peierls-like mechanism. We may therefore state that, in the strong correlation limit, the MIT of this material is due to the orbital ordering instability hidden in the single trellis layer. The double trellis layer on the other hand becomes Mott insulating due to the charge flow, as we have already discussed in Secs. IIIB and IIIC. We hope that any experimental confirmation of the orbital ordering pattern predicted here would justify the validity of the present scenario for the MIT of this material.

IV. SUMMARY

We have carried out the DFT-based electronic-structure calculations of a Wadsley-phase vanadium oxide V_6O_{13} and have clarified its electronic structure of both the high-temperature metallic and low-temperature insulating phases. We have thereby considered the mechanism of the observed MIT and antiferromagnetic transition.

We have shown the following: In the high-temperature metallic phase, an electron is located largely on the d_{xz} orbital of V(1) with a substantial admixture of the d_{yz} orbital, and other two electrons are located largely on the d_{xy} orbitals of V(3) with a significant contribution from the d_{xy} orbital of V(2). Two sets of the quasi-1D Fermi surfaces are formed by the two nearly degenerate bands coming from the d_{xy} orbitals of V(2) and V(3), and the quasi-2D-like Fermi surface is formed by the band coming from the d_{yz} orbital of V(1). Further experimental studies determining the band structure near the Fermi level, such as the ARPES experiment with high resolution, are desirable to confirm the validity of our

theoretical predictions for the high-temperature metallic phase of V_6O_{13} .

In the low-temperature insulating phase, there appears the band gap, the size of which is consistent with the experimental value for an appropriate choice of the U value. We find that the redistribution of electrons occurs at the MIT, which leads to the oxidation states of V^{4+} ($3d^1$) for the V(1) and V(3) ions and V^{5+} ($3d^0$) for the V(2) ions. More precisely, an electron is localized on each of the d_{xz} orbital of V(1a) and d_{yz} orbital of V(1b) in the single trellis layer, and an electron is localized on each of the d_{xy} orbitals of V(3a) and V(3b) in the double trellis layer. The orbital and charge orderings associated with the MIT thus occur in the low-temperature insulating phase of V_6O_{13} .

We have then discussed that, in consequence of these charge and orbital orderings, the two electrons on the neighboring V(1a) and V(1b) ions in the single trellis layer form the spin-singlet state, and therefore the spin excitations are suppressed at temperatures below the MIT in agreement with experiment. The electrons on the d_{xy} orbitals of the V(3a) and V(3b) ions in the double trellis layers, on the other hand, undergo the Mott transition to form the quasi-1D zigzag ladders of $S = \frac{1}{2}$ spins with strong frustration, and may be responsible for the antiferromagnetic long-range order observed below 55 K. Thus, the spin-singlet and antiferromagnetic states coexist in spatially separated regions of this material at lowest temperatures.

We have suggested a possible scenario that the MIT of this system is caused by the band Jahn-Teller-type instability, or the orbital ordering instability in the strong correlation limit, which is hidden in the zigzag ladder of the V(1) ions in the single trellis layer. Further experimental studies, including the confirmation of the predicted orbital ordering pattern as well as the determination of the antiferromagnetic spin structure and excitations, are desirable for drawing definite conclusions on the mechanism of the MIT and low-temperature electronic states of V_6O_{13} .

ACKNOWLEDGMENTS

We thank M. Itoh, Y. Shimizu, and Y. Ueda for enlightening discussions on the experimental aspects of V_6O_{13} and S. Nishimoto for informative discussions on the theoretical aspects. This work was supported in part by Futaba Electronics Memorial Foundation and by Grants-in-Aid for Scientific Research (Grant Nos. 22540363 and 26400349) from JSPS of Japan. T.T. acknowledges support from the JSPS Research Fellowship for Young Scientists.

-
- [1] N. F. Mott, *Metal-Insulator Transitions*, 2nd ed. (Taylor & Francis, London, 1990).
 - [2] S. Kachi, K. Kosuge, and H. Okinaka, *J. Solid State Chem.* **6**, 258 (1973).
 - [3] K. Kawashima, Y. Ueda, K. Kosuge, and S. Kachi, *J. Crystal Growth* **26**, 321 (1974).
 - [4] A. C. Gossard, F. J. Di Salvo, L. C. Erich, J. P. Remeika, H. Yasuoka, K. Kosuge, and S. Kachi, *Phys. Rev. B* **10**, 4178 (1974).
 - [5] P. D. Dernier, *Mater. Res. Bull.* **9**, 955 (1974).
 - [6] Y. Ueda, K. Kosuge, and S. Kachi, *Mater. Res. Bull.* **11**, 293 (1976).
 - [7] B. Fisher and A. Ron, *Solid State Commun.* **40**, 737 (1981).
 - [8] M. Itoh, H. Yasuoka, Y. Ueda, and K. Kosuge, *J. Phys. Soc. Jpn.* **53**, 1847 (1984).
 - [9] M. Onoda, T. Ohki, and Y. Uchida, *J. Phys.: Condens. Matter* **16**, 7863 (2004).
 - [10] K.-A. Wilhelmi, K. Waltersson, and L. Kihlberg, *Acta Chem. Scand.* **25**, 2675 (1971).

- [11] I. Kawada, M. Ishii, M. Saeki, N. Kimizuka, M. Nakano-Onoda, and K. Kato, *Acta Crystallogr. B* **34**, 1037 (1978).
- [12] J. Höwing, T. Gustafsson, and J. O. Thomas, *Acta Crystallogr. B* **59**, 747 (2003).
- [13] Y. Ueda *et al.* (private communication).
- [14] S. Shin, S. Suga, M. Taniguchi, M. Fujisawa, H. Kanzaki, A. Fujimori, H. Daimon, Y. Ueda, K. Kosuge, and S. Kachi, *Phys. Rev. B* **41**, 4993 (1990).
- [15] S. Suga, A. Sekiyama, M. Obara, J. Yamaguchi, M. Kimura, H. Fujiwara, A. Irizawa, K. Yoshimura, M. Yabashi, K. Tamasaku, A. Higashiya, and T. Ishiwaka, *J. Phys. Soc. Jpn.* **79**, 044713 (2010).
- [16] R. Eguchi, T. Yokoya, T. Kiss, Y. Ueda, and S. Shin, *Phys. Rev. B* **65**, 205124 (2002).
- [17] S. Suga, A. Shigemoto, A. Sekiyama, S. Imada, A. Yamasaki, A. Irizawa, S. Kasai, Y. Saitoh, T. Muro, N. Tomita, K. Nasu, H. Eisaki, and Y. Ueda, *Phys. Rev. B* **70**, 155106 (2004).
- [18] T. Schmitt, L.-C. Duda, M. Matsubara, M. Mattesini, M. Klemm, A. Augustsson, J.-H. Guo, T. Uozumi, S. Horn, R. Ahuja, A. Kotani, and J. Nordgren, *Phys. Rev. B* **69**, 125103 (2004).
- [19] M. Itoh, I. Yamauchi, T. Kozuka, T. Suzuki, T. Yamauchi, J.-I. Yamaura, and Y. Ueda, *Phys. Rev. B* **74**, 054434 (2006).
- [20] T. Suzuki, I. Yamauchi, Y. Shimizu, M. Itoh, N. Takeshita, C. Terakura, H. Takagi, Y. Tokura, T. Yamauchi, and Y. Ueda, *Phys. Rev. B* **79**, 081101(R) (2009).
- [21] P. Blaha, K. Schwarz, G. K. H. Madsen, D. Kvasnicka, and J. Luitz, *Wien2k, An Augmented Plane Wave Plus Local Orbitals Program for Calculating Crystal Properties* (Technische Universität Wien, Austria, 2001).
- [22] V. I. Anisimov, I. V. Solovyev, M. A. Korotin, M. T. Czyżyk, and G. A. Sawatzky, *Phys. Rev. B* **48**, 16929 (1993).
- [23] A. I. Liechtenstein, V. I. Anisimov, and J. Zaanen, *Phys. Rev. B* **52**, R5467 (1995).
- [24] J. P. Perdew, K. Burke, and M. Ernzerhof, *Phys. Rev. Lett.* **77**, 3865 (1996).
- [25] G. Kotliar, S. Savrasov, K. Haule, V. Oudovenko, O. Parcollet, and C. Marianetti, *Rev. Mod. Phys.* **78**, 865 (2006).
- [26] K. Held, *Adv. Phys.* **56**, 829 (2007).
- [27] M. Imada and T. Miyake, *J. Phys. Soc. Jpn.* **79**, 112001 (2010).
- [28] V. Anisimov and Y. Izyumov, *Electronic Structure of Strongly Correlated Materials*, Springer Series in Solid-State Sciences Vol. 163 (Springer, Heidelberg, 2010).
- [29] *The LDA + DMFT Approach to Strongly Correlated Materials*, edited by E. Pavarini, E. Koch, D. Vollhardt, and A. Lichtenstein (Forschungszentrum Jülich GmbH, Jülich, 2011).
- [30] F. Tran and P. Blaha, *Phys. Rev. Lett.* **102**, 226401 (2009).
- [31] K. Momma and F. Izumi, *J. Appl. Crystallogr.* **41**, 653 (2008).
- [32] A. Kokalj, *Comput. Mater. Sci.* **28**, 155 (2003).
- [33] T. Aoyama, Y. Shimizu, T. Jinno, M. Itoh, and Y. Ueda (unpublished).
- [34] M. Isobe and Y. Ueda, *J. Phys. Soc. Jpn.* **65**, 1178 (1996).
- [35] T. Ohama, H. Yasuoka, M. Isobe, and Y. Ueda, *Phys. Rev. B* **59**, 3299 (1999).
- [36] H. Seo and H. Fukuyama, *J. Phys. Soc. Jpn.* **67**, 2602 (1998).
- [37] S. Nishimoto and Y. Ohta, *J. Phys. Soc. Jpn.* **67**, 2996 (1998).
- [38] H. T. Lu, Y. J. Wang, S. Qin, and T. Xiang, *Phys. Rev. B* **74**, 134425 (2006).
- [39] S. Nishimoto, K. Sano, and Y. Ohta, *Phys. Rev. B* **77**, 085119 (2008), and references therein.
- [40] S. R. White and I. Affleck, *Phys. Rev. B* **54**, 9862 (1996).
- [41] F. Monti and A. Sütő, *Phys. Lett. A* **156**, 197 (1991); *Helv. Phys. Acta* **65**, 560 (1992).